Current-Driven Plasma Acceleration Versus Current-Driven Energy Dissipation
Part II: Electromagnetic Wave Stability Theory and Experiments*

E.Y. Choueiri†, A.J. Kelly‡and R.G. Jahn.§

Electric Propulsion and Plasma Dynamics Laboratory
Princeton University, Princeton, NJ 08544, USA

Abstract

A theoretical/experimental study of the dominant unstable wave modes of an electromagnetically accelerated plasma is presented. The study is the second part of a three-phase investigation aimed at characterizing the current-driven microinstabilities behind the turbulent dissipation degrading the efficiency of the MPD accelerator. The analysis uses a kinetic theory that combines all the features of our previous models with the addition of one new effect, namely, the allowance for electromagnetic modes necessitated by the finite plasma beta (ratio of thermal to magnetic pressures). A fully electromagnetic dielectric tensor is derived for a magnetoactive, current-carrying, collisional and finite-beta flowing plasma. We have used, elsewhere, this dielectric tensor to investigate in detail the dominant unstable modes of the MPD accelerator plasma as well as to derive the corresponding anomalous transport coefficients. In this paper our aim is the use of the stability theory to interpret experiments. Experiments were conducted under conditions where the measured current is substantially larger than diamagnetic drift currents so that the effects of gradients can be neglected. The experiments included plasma characterization measurements and plasma wave measurements. The measured dispersion relation and growth rates were in general agreement with the theory. The frequency of the dominant unstable mode was, as predicted, near the lower hybrid frequency.

*This work is supported by the National Aeronautics and Space Administration under contract NASA-954997 and the Air Force Office of Scientific Research under contract AFOSR-91-0162 and DOE/Princeton Plasma Physics Laboratory.

†Research Associate.

‡Senior Research Staff.

§Professor.

1 Introduction

The microstability of an electromagnetically accelerated plasma, such as that of the MPD accelerator, is a problem that has, until recently, received very little attention in the literature. This is so, even though various scattered experimental, analytical and numerical studies have repeatedly hinted at the importance of plasma collective effects (waves, instabilities and turbulence) in dissipating energy otherwise available to the acceleration process. A review of the studies to-date that have directly or indirectly addressed microinstabilities and microturbulence and their manifestation in the context of such plasmas has recently been made in ref. [1]. All of the few previous theoretical studies that were concerned with microinstabilities in the MPD accelerator plasma were done under the electrostatic assumption and none have been directly compared to wave experiments.

Our approach to the problem of instability-driven dissipation in the MPD accelerator consists of two research programs. First is a plasma physics program in which the nature, dependences and effects of microinstability and turbulence are studied both theoretically and experimentally to arrive at working models for turbulent transport. Second is an engineering program in which these transport models are coupled to the flow through self-consistent fluid codes which can be used to optimize the design and/or the operation conditions of real MPD accelerators for high thrust efficiency as well as experiments to test the validity of the optimizing solutions. While the engineering program has just started with the fluid code simulations reported in ref. [2], the goals of the plasma physics program have been largely accomplished as documented fully in ref. [1] and partly in this paper.

This program, in turn, consists of three phases.

First is the theoretical investigation of the microinstabilities with the goal of identifying the dominant wave modes given the accelerator plasma state. The ultimate tool for such a study is a kinetic description of the dielectric response of the plasma to linear oscillations including as much relevant physics as possible. The second phase is the corroboration of the identified modes with wave experiments through either active excitation of linear oscillations or passive monitoring of saturated oscillations. Once a certain confidence in the capability of the kinetic theory to describe the linear growth stage of unstable modes is reached one can proceed to study the effects of the identified microinstabilities on the plasma and the dissipation energetics. In this third phase the goal is to model and study the nonlinear effects of the resulting microturbulence on the transport in the plasma.

While the first phase of the program outlined above was documented (in the electrostatic limit) in ref. [3] which is Part I of this series of papers, the present paper addresses the second phase, namely the correlation between our most recent and encompassing theoretical description of waves and instabilities in the MPD accelerator and wave experiments conducted within the discharge.

We start, in the following section, by outlining the derivation of our most recent theory of microinstabilities in the MPD accelerator plasma. The theory uses a kinetic description that includes magnetic and thermal effects as well as those of an electron current transverse to the magnetic field and collisions, thus combining all the features of our previous models with the addition of one new effect, namely, the allowance for electromagnetic modes. Electromagnetic wave effects must be considered in the stability analysis because of the finite plasma beta (ratio of thermal to magnetic pressures) of the accelerator plasma. A fully electromagnetic dielectric tensor for the plasma is derived from first principles in the ion reference frame including the effects of electron collisions. The dielectric tensor also contains the full electromagnetic response of the ions and the contribution of the electron cyclotron harmonics. The neglect of these two effects, commonly done in the literature, can under some conditions lead to qualitatively erroneous descriptions as demonstrated in recent studies.

Unlike the detailed theoretical study of Part I (ref. [3]) where we solved the purely electrostatic dispersion relation for various combinations of the governing parameters and explored the various properties of the dominant electrostatic modes, we will not seek, in this paper, the exploration of the parameter-space with the more complicated electromagnetic dispersion relation presented here. The goal here is rather to compare the theory to experimental measurements. The reader interested in microinstability characterization studies is referred to the detailed analysis in ref. [1] where the full dispersion relation is used to study the nature, characteristics, threshold criteria, polarization of the dominant modes and the effects of collisions and spatial evolution as well as the use of the theory in the weak turbulence formalism to derive anomalous transport rates.

(It is sufficient, for the purposes of this paper, to state that the dominant instability found in that study was termed "Lower Hybrid Current Driven Instability" (LHCDI) and is a particular case of the "Generalized Lower Hybrid Drift Instability" (GLHDI). The instability is akin to the modified two-stream instability (MTSI) but with important finite-beta (electromagnetic) amendments. The electrostatic branch of LHCDI was investigated extensively in Part I of our study[3]. The electromagnetic amendments to the electrostatic mode consisted primarily of shifting the maximum growth rates to more oblique propagation (with respect to the local magnetic field) and a relative damping of the modes. These effects were attributed to the coupling of the lower hybrid wave with a pseudo-whistler wave. The unstable waves were found to have finite polarization and cause considerable disturbance to the magnetic field.)

The second part of this paper is concerned with the comparison of both the real and imaginary parts of the theoretical dispersion relation with experiments. These experiments were specifically designed with the theory's limitations in mind. Still, some of the assumptions of the theory are hard to reconcile with experimental reality and are discussed in some detail. The experimental wave data are normalized using the locally measured plasma parameters and compared to the theoretical dispersion.

2 The Dispersion Tensor of a Current-Carrying, Collisional, and Flowing Plasma

We now seek a general kinetic description of the response of a collisional and flowing magnetoactive plasma carrying a cross-field current to small perturbations without making the electrostatic assumption.

2.1 Stating the Problem

Our entire problem can be formulated, as shown below, to be contained in the following matrix equation

$$\begin{pmatrix} R_{xx} & R_{xy} & R_{xz} \\ R_{yx} & R_{yy} & R_{yz} \\ R_{zx} & R_{zy} & R_{zz} \end{pmatrix} \begin{pmatrix} E_x^{(1)} \\ E_y^{(1)} \\ E_z^{(1)} \end{pmatrix} = 0 \qquad (1)$$

where the superscript 1 denotes the first order harmonic part of the linearly perturbed quantities (in this case, the components of the electric field vector $\boldsymbol{E}$). In the above equation, R_{ij} represent the elements of the *dispersion tensor* $\boldsymbol{R}(\omega, \boldsymbol{k})$ and are generally complex functions of the frequency ω and wavevector $\boldsymbol{k}$ of the oscillations as well as of all the plasma parameters of the problem. All the phase and amplitude information pertaining to the dispersion of the waves can be found in the solution of the following equation that results from the condition for non-trivial solution to the above set of homogeneous equations,

$$\det|R_{ij}(\omega, \boldsymbol{k})| = 0, \qquad (2)$$

which states that the determinant of the dispersion tensor must vanish. For a given set of parameters the above equation relates the frequency and growth of the oscillation to the wavenumber and is called the *dispersion relation*. Once a root of the dispersion relation is found (we shall only be concerned with the root with the largest growth rate) more information concerning the polarization of the oscillating electric and magnetic fields can be obtained by going back to Eq. (1) and solving for the electric field. All this information is very valuable for the identification of the unstable modes of the plasma.

In this section we outline the derivation of explicit expressions for the elements R_{ij} needed for our study. More details on the derivation can be found in ref. [1].

2.2 Defining the Problem in Terms of the Conductivity, Dielectric and Dispersion Tensors

The conductivity tensor $\boldsymbol{\sigma}$ and the dielectric tensor $\boldsymbol{K}$ are defined by

$$\boldsymbol{j}^{(1)} = \boldsymbol{\sigma}\boldsymbol{E}^{(1)} \qquad (3)$$

$$\boldsymbol{K}\boldsymbol{E}^{(1)} = \boldsymbol{E}^{(1)} + \frac{i}{\epsilon_0\omega}\boldsymbol{j}^{(1)}. \qquad (4)$$

By eliminating the perturbed current density vector, $\boldsymbol{j}^{(1)}$ from the above definitions we get

$$K_{ij} = \delta_{ij} + \frac{i\sigma_{ij}}{\epsilon_0\omega} \qquad (5)$$

where δ_{ij} is Kronecker's delta representing the identity tensor. If we now recall two of Maxwell's linearized equations

$$\boldsymbol{k} \times \boldsymbol{E^{(1)}} = \omega \boldsymbol{B^{(1)}} \qquad (6)$$

$$i\boldsymbol{k} \times \boldsymbol{B^{(1)}} = \mu_0 \boldsymbol{j^{(1)}} - i\mu_0\epsilon_0\omega \boldsymbol{E^{(1)}} \qquad (7)$$

and eliminate the perturbed magnetic field vector $\boldsymbol{B^{(1)}}$ from the second equation using the first, we obtain after dividing by k^2 and using Eq. (4)

$$N^2 \left(\frac{\boldsymbol{k} \times (\boldsymbol{k} \times \boldsymbol{E}^{(1)})}{k^2} + \boldsymbol{K}\boldsymbol{E}^{(1)} \right) = 0 \qquad (8)$$

which can be written in the form of Eq. (1),

$$\boldsymbol{R}\boldsymbol{E}^{(1)} = 0 \qquad (9)$$

where we identify $\boldsymbol{R}$ as the dispersion tensor whose elements can now be written in terms of those of the dielectric tensor or, more conveniently, through Eq. (5), in terms of those of the conductivity tensor

$$R_{ij} = N^2 \left(\frac{k_i k_j}{k^2} - \delta_{ij} \right) + \delta_{ij} + \frac{i\sigma_{ij}}{\epsilon_0\omega} \qquad (10)$$

where

$$N \equiv \frac{ck}{\omega} \qquad (11)$$

is the index of refraction.

In order to arrive at the sought expressions for R_{ij} we shall invoke plasma kinetic theory to find a relation between the current density and the electric field which we shall put in the form of Eq. (3) thus allowing us to write the dispersion tensor explicitly through Eq. (10).

2.3 Derivation of the Perturbed Distribution Function

Our starting point for formulating a kinetic prescription relating the perturbed current density vector to the electric field is the Vlasov equation with the collisions represented by the BGK model[4],

$$\begin{aligned} &\frac{\partial f_s}{\partial t} + \boldsymbol{v} \cdot \nabla_{\boldsymbol{x}} f_s \\ &\quad + \frac{q_s}{m_s} \left[\boldsymbol{E}(\boldsymbol{x}, t) + \boldsymbol{v} \times \boldsymbol{B} \right] \cdot \nabla_{\boldsymbol{v}} f_s(\boldsymbol{x}, \boldsymbol{v}, t) \\ &\quad = -\nu_s (f_s - \frac{n_s}{n_s^{(0)}} f_s^{(0)}). \end{aligned} \qquad (12)$$

where q_s, m_s, f_s, ν_s are the charge, mass, velocity distribution function and collision frequency of species s

respectively. We now linearize by assuming that all quantities with spatial and temporal dependences, $\boldsymbol{E}, \boldsymbol{B}, f_s, \boldsymbol{j}$ and the charge density ρ are perturbed about their steady-state values (superscripted with 0) by harmonic quantities (superscripted with 1) so that for a generic quantity a we have

$$a = a^{(0)} + a^{(1)} \tag{13}$$

and $|a^{(1)}/a^{(0)}| \ll 1$. After replacing the temporal and spatial differential operators by $-i\omega$ and $i\boldsymbol{k}$ respectively, the linearization of Eq. (12) results in the following expression for the perturbed distribution function

$$-i(\omega + i\nu_s - \boldsymbol{k}\cdot\boldsymbol{v})f_s^{(1)} + \frac{q_s}{m_s}\left(\boldsymbol{v}\times\boldsymbol{B^{(0)}}\right)\cdot\nabla_{\boldsymbol{v}} f_s^{(1)} = -\frac{q_s}{m_s}\left(\boldsymbol{E^{(1)}} + \boldsymbol{v}\times\boldsymbol{B^{(1)}}\right)\cdot\nabla_{\boldsymbol{v}} f_s^{(0)} + \nu_s\frac{n_s^{(1)}}{n_s^{(0)}}f_s^{(0)} \tag{14}$$

If we choose to work with the cylindrical phase space coordinates, $v_\perp, \phi, v_z$, with the magnetic field aligned with the z-axis the above equation can be recast into a first order linear inhomogeneous differential equation in $f_s^{(1)}$ which can be integrated once to yield

$$f_s^{(1)} = \frac{1}{\Upsilon(\phi)\omega_{cs}}\int \Upsilon(\phi) \times\left\{\frac{q_s}{m_s}\left[\boldsymbol{E^{(1)}} + \frac{(\boldsymbol{v}\cdot\boldsymbol{E^{(1)}})\boldsymbol{k} - (\boldsymbol{k}\cdot\boldsymbol{v})\boldsymbol{E^{(1)}}}{\omega}\right]\cdot\nabla_{\boldsymbol{v}} f_s^{(0)} + \nu_s\frac{n_s^{(1)}}{n_s^{(0)}}f_s^{(0)}\right\}d\phi + C \tag{15}$$

where the integrating factor $\Upsilon(\phi)$ can be written as

$$\Upsilon(\phi) = \exp\left[i\frac{\omega + i\nu_s - k_z v_z}{\omega_{cs}}\phi\right] \times\sum_{n=-\infty}^{\infty} i^n J_n\left(\frac{k_\perp v_\perp}{\omega_{cs}}\right)e^{in\phi}, \tag{16}$$

where $J_n(a)$ is the Bessel function of integer order n and we have chosen, without any loss of generality, the wavevector to be in the y-z plane as shown in Fig. (1), namely

$$\boldsymbol{k} = (0, k_\perp, k_z). \tag{17}$$

We now introduce the steady-state distribution function $f_s^{(0)}$. Since we are interested in a description that can be easily used to interpret data acquired from probes immersed in the flowing plasma but stationary in the laboratory frame, we shall carry our derivation in the laboratory frame by allowing cross-field drifts in both the ion and electron distribution functions. For a cross-field drift in a homogeneous flowing plasma the steady-state distribution function is a drifting Maxwellian

$$f_s^{(0)}(\boldsymbol{v}) = \left(\frac{m_s}{2\pi T_s}\right)^{3/2} \times\exp\left[-\frac{m_s}{2T_s}\left(v_x^2 + (v_y - u_{ds})^2 + v_z^2\right)\right] \tag{18}$$

where u_{ds} and T_s are the cross-field drift velocity and temperature of species s in the laboratory frame and is taken to be aligned along the y-axis as shown in Fig. (1).

Upon substituting the above expression and Eq. (16) in Eq. (15), integrating over the azimuthal angle and using the following recursive relations

$$J_{n-1}(a) + J_{n+1}(a) = 2\frac{n}{a}J_n(a) \tag{19}$$

$$J_{n-1}(a) - J_{n+1}(a) = 2J_n'(a), \tag{20}$$

where the prime denotes the derivative with respect to the argument, we obtain

$$f_s^{(1)} = \frac{iq_s}{\omega T_s}(\omega - k_\perp u_{ds})f_s^{(0)} \times\frac{e^{-in\phi}\sum_{m=-\infty}^{\infty} i^m J_m\left(k_\perp v_\perp/\omega_{cs}\right)e^{im\phi}}{\omega + i\nu_s + n\omega_{cs} - k_z v_z - k_\perp u_{ds}} \times\left\{\boldsymbol{C_n}\cdot\boldsymbol{E^{(1)}} + \nu_s\frac{n_s^{(1)}T_s}{n_s^{(0)}q_s}J_n\right\} \tag{21}$$

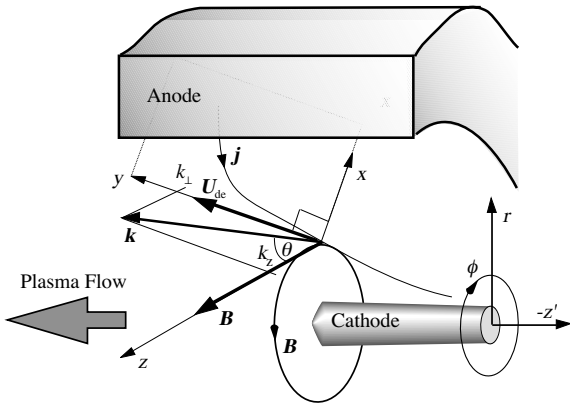

Figure 1: The vectors $\boldsymbol{j}$, $\boldsymbol{B}$, $\boldsymbol{k}$ and $\boldsymbol{u_{de}}$ in the local cartesian coordinate frame. Also shown is the accelerator's fixed cylindrical coordinate frame, r-z'-θ.

where the vector of coefficients $\boldsymbol{C_n}$ is defined as

$$\boldsymbol{C_n} \equiv iv_\perp J_n' \hat{e}_x + \left(v_{ds} - \frac{n\omega_{cs}}{k_\perp} \right) J_n \hat{e}_y + v_z J_n \hat{e}_z. \quad (22)$$

2.4 Switching to the Potential Formalism

We shall now abandon the electric field formalism exemplified in Eq. (1) in favor of a formalism cast in terms of the electrostatic and electromagnetic potentials, Φ and $\boldsymbol{A}$ defined below. This has three advantages. The first advantage is a clear separation of electromagnetic and electrostatic effects in the dispersion tensor making it more natural to a discussion of electromagnetic correction to an electrostatic mode[5]. This will be especially advantageous in the context of the anomalous transport theory that we developed in ref. [1] and used in ref. [2] where it is insightful to separate the electrostatic and electromagnetic contributions to the anomalous heating and momentum exchange rates. The second advantage is the fact that, in the case where the ions are taken to be unmagnetized, their contribution to the dispersion tensor is much tidier mathematically than in the electric field formalism. Finally, the third advantage is that the effects of collisions on the purely electromagnetic modes can be simply prescribed in the potential formalism.

The electromagnetic potential $\boldsymbol{A}$ is defined by

$$\boldsymbol{B} = \nabla \times \boldsymbol{A}. \quad (23)$$

Any arbitrary choice of $\boldsymbol{A}$ of the form $\boldsymbol{A} + \nabla\psi$ (where ψ is single valued) is, in general, possible. This "arbitrariness of gauge", as it is customarily called in electrodynamics, is most appropriately removed by imposing the Coulomb gauge $\nabla \cdot \boldsymbol{A} = 0$. Rewriting the "$\nabla \times \boldsymbol{E}$" Maxwell equation using the above definition we get

$$\nabla \times \left(\boldsymbol{E} + \frac{\partial \boldsymbol{A}}{\partial t} \right) = 0 \quad (24)$$

which implies that the quantity $(\boldsymbol{E} + \frac{\partial \boldsymbol{A}}{\partial t})$ can be represented by a potential gradient $-\nabla\Phi$, and for linear harmonic perturbations we thus have

$$\boldsymbol{E^{(1)}} = i\omega \boldsymbol{A^{(1)}} - i\boldsymbol{k}\Phi^{(1)}. \quad (25)$$

Taking the divergence of the electric field, using the corresponding Maxwell equation and the Coulomb gauge we also get

$$\Phi^{(1)} = \frac{\rho^{(1)}}{\epsilon_0 k^2}. \quad (26)$$

Finally, upon substituting Eqs. (25) and (23) in Maxwell's "$\nabla \times \boldsymbol{B}$" equation, the following relation results

$$\left(k^2 - \frac{\omega^2}{c^2} \right) \boldsymbol{A^{(1)}} - \frac{\omega}{c^2} \boldsymbol{k}\Phi^{(1)} = \mu_0 \boldsymbol{j}^{(1)}. \quad (27)$$

The above two equations become specified once expressions for the perturbed charge and current densities, $\rho^{(1)}$ and $\boldsymbol{j}^{(1)}$, are found in terms of $\boldsymbol{A^{(1)}}$ and $\Phi^{(1)}$. This will be done using the following moments

$$\rho^{(1)} = \sum_s q_s \int f_s^{(1)} d^3\boldsymbol{v}, \quad (28)$$

$$\boldsymbol{j}^{(1)} = \sum_s q_s \int f_s^{(1)} \boldsymbol{v} d^3\boldsymbol{v} \quad (29)$$

so that Eqs. (26) and (27) can be written as a set of three homogeneous equations in $\Phi^{(1)}$, $A_x^{(1)}$ and $A_z^{(1)}$ (and we have eliminated $A_y^{(1)}$ with the Coulomb gauge)

$$\begin{pmatrix} D_{11} & D_{12} & D_{13} \\ D_{21} & D_{22} & D_{23} \\ D_{31} & D_{32} & D_{33} \end{pmatrix} \begin{pmatrix} \Phi^{(1)} \\ A_x^{(1)} \\ A_z^{(1)} \end{pmatrix} = 0 \quad (30)$$

The above matrix equation and the dispersion tensor D_{ij} are the analogs of Eq. (1) and the tensor R_{ij}, respectively, in the potential formalism.

The perturbed distribution function $f_s^{(1)}$ needed to take the moments in Eqs. (28) and (29) and close the system can now be rewritten in the potential formalism

$$f_s^{(1)} = \frac{iq_s}{\omega T_s}(\omega - k_\perp u_{ds}) f_s^{(0)} \times \frac{e^{-in\phi} \sum_{m=-\infty}^{\infty} i^m J_m(k_\perp v_\perp/\omega_{cs})\, e^{im\phi}}{\omega + i\nu_s + n\omega_{cs} - k_z v_z - k_\perp u_{ds}} \times \left\{ \boldsymbol{C_n} \cdot (i\omega \boldsymbol{A^{(1)}} - i\boldsymbol{k}\Phi^{(1)}) + \nu_s \frac{\boldsymbol{k} \cdot \boldsymbol{j}_s^{(1)} T_s}{\omega q_s^2 n_s^{(0)}} J_n \right\} \quad (31)$$

where we have also eliminated $n_s^{(1)}$ in favor of $j_s^{(1)}$ using

$$n_s^{(1)} = \frac{\boldsymbol{k} \cdot \boldsymbol{j}_s^{(1)}}{\omega q_s} \quad (32)$$

which can be directly obtained by taking the divergence of Maxwell's "$\nabla \times \boldsymbol{B}$" equation.

2.5 The Resulting Dispersion Tensor

Our last task is to carry the velocity space integration required by the moments in Eqs. (28) and (29)

using the above expression for $f_s^{(1)}$. The integration is carried in cylindrical velocity coordinates and thus takes the form

$$\int d^3\boldsymbol{v} = \int_0^\infty v_\perp\, dv_\perp \int_{-\infty}^{\infty} dv_z \int_0^{2\pi} d\phi. \quad (33)$$

After the integration over ϕ the parallel velocity integrals are of the form

$$\int_{-\infty}^{\infty} G(v_z) \frac{v_z^p}{\omega + i\nu_s + n\omega_{cs} - k_z v_z - k_\perp u_{ds}} dv_z \quad (34)$$

where $p = 0, 1, 2$. These integrals can be expressed as linear functions of the well known plasma dispersion function

$$Z(\zeta_s) \equiv \frac{1}{\sqrt{\pi}} \int_{-\infty}^{\infty} \frac{e^{-t^2}}{t - \zeta_s}\, dt \quad (35)$$

and its derivative with respect to its argument. The integration over the perpendicular velocity transforms the Bessel functions into modified Bessel functions, $I_n(\mu_s)$ of the first kind and of integer order n with the argument being the square of the normalized perpendicular wavelength $\mu_s \equiv k_\perp^2 r_{cs}^2/2$.

After much tedious algebra, where we use the following relations

$$\frac{dZ}{d\zeta_s} = -2(1 + \zeta_s Z) \quad (36)$$

$$\sum_{n=-\infty}^{\infty} n I_n(\mu_s) = 0, \quad \sum_{n=-\infty}^{\infty} I_n(\mu_s) = e^{\mu_s}, \quad (37)$$

$$\sum_{n=-\infty}^{\infty} n^2 I_n(\mu_s) = \mu_s e^{\mu_s} \quad (38)$$

and, as in our previous studies, assume the ions to be unmagnetized but keep in full their electromagnetic contribution (which has been recently demonstrated in ref. [6] to be important) and neglect the ion collisions, the elements of the dispersion tensor D_{ij} can finally be written explicitly in terms of the wave and plasma parameters

$$D_{11} = 1 + \alpha_i(1 + \zeta_i Z_i) + \alpha_e \left(\frac{1 + \zeta_{e0} e^{-\mu_e} \sum_{n=-\infty}^{\infty} I_n Z_{en}}{1 + i(\nu_e/k_z v_{te}) e^{-\mu_e} \sum_{n=-\infty}^{\infty} I_n Z_{en}} \right) \quad (39)$$

$$D_{12} = -i \frac{\omega_{pe}^2}{\tilde{\omega}^2} \frac{k_z}{k} \zeta_{e0} \sqrt{2\mu_e} e^{-\mu_e} \times \sum_{n=-\infty}^{\infty} (I_n - I_n')(1 + \tilde{\zeta}_{e0} Z_{en}) \quad (40)$$

$$D_{13} = 2 \frac{\omega_{pe}^2}{\tilde{\omega}^2} \frac{k_z}{k} \zeta_{e0} e^{-\mu_e} \times \sum_{n=-\infty}^{\infty} I_n \left\{ \vartheta_n^2 Z_{en} + \left[\left(\frac{u_{de}}{v_{te}} \right)^2 / \zeta_{e0} \right] + (1 + \zeta_{en} Z_{en}) \left(\vartheta_n \frac{k_\perp^2 - k_z^2}{k_\perp k_z} - \zeta_{en} \right) \right\} \quad (41)$$

$$D_{22} = 1 - N^2 + \frac{\omega_{pi}^2}{\omega^2} \zeta_i Z_i + \frac{\omega_{pe}^2}{\tilde{\omega}^2} \zeta_{e0} \mu_e e^{-\mu_e} \times \sum_{n=-\infty}^{\infty} \left[\frac{n^2}{\mu_e^2} I_n + 2(I_n - I_n') \right] Z_{en} \quad (42)$$

$$D_{23} = -i \frac{\omega_{pe}^2}{\tilde{\omega}^2} \zeta_{e0} \sqrt{2\mu_e} e^{-\mu_e} \sum_{n=-\infty}^{\infty} (I_n - I_n') \times \left[1 + \left(\frac{k_z}{k_\perp} \vartheta_n + \zeta_{en} \right) Z_{en} \right] \quad (43)$$

$$D_{33} = 1 - N^2 + \frac{\omega_{pi}^2}{\omega^2} \zeta_i Z_i + 2 \frac{\omega_{pe}^2}{\tilde{\omega}^2} \frac{k_\perp^2}{k^2} \left[\left(\zeta_{e0} - \frac{k_z}{k_\perp} \frac{u_{de}}{v_{te}} \right)^2 + \zeta_{e0} e^{-\mu_e} \times \sum_{n=-\infty}^{\infty} I_n Z_{en} \left(\frac{k_z}{k_\perp} \vartheta_n + \zeta_{en} \right)^2 \right] \quad (44)$$

$$D_{21} = -D_{12}; \quad D_{31} = \frac{k_\perp^2}{k^2} D_{13} \quad (45)$$

$$D_{32} = -\frac{k_\perp^2}{k^2} D_{23} \quad (46)$$

where we have used the following definitions

$$\zeta_{en} \equiv \frac{\omega + n\omega_{ce} - k_\perp u_{de} + i\nu_e}{k_z v_{te}}; \quad \zeta_i \equiv \frac{\omega - k_\perp u_f}{k v_{ti}}; \quad (47)$$

$$\tilde{\omega} \equiv \omega + i\nu_e; \quad \tilde{\zeta}_{e0} \equiv \frac{\tilde{\omega}}{k_z v_{te}} = \zeta_{e0} + \frac{k_\perp}{k_z} \frac{u_{de}}{v_{te}}; \quad (48)$$

$$\vartheta_n \equiv \frac{k_z}{k_\perp} (\zeta_{en} - \tilde{\zeta}_{e0}); \; Z_{en} \equiv Z(\zeta_{en}); \; I_n \equiv I_n(\mu_e). \quad (49)$$

and the thermal velocity, plasma frequency and cyclotron frequency of species s are, respectively, given by

$$v_{ts} = (2T_s/m_s)^{1/2}; \; \omega_{ps} \equiv \left(\frac{q_s^2 n_{0_s}}{\epsilon_0 m_s} \right)^{1/2}; \; \omega_{cs} \equiv \frac{q_s B_0}{m_s}. \quad (50)$$

It is also useful to note that the refraction index N appearing in the above dispersion tensor can be related to the plasma parameters through the following relation

$$N^2 \equiv \frac{c^2 k^2}{\omega^2} = 2 \frac{\omega_{pi}^2}{\omega^2} \frac{\mu_e}{\beta_e} \frac{m_i}{m_e} \frac{k^2}{k_\perp^2} \quad (51)$$

where we have introduced β_s, the beta of species s, (s in the above equation is set to e for electrons) defined as the ratio of thermal pressure to magnetic pressure

$$\beta_s \equiv \frac{n_s k T_s}{B_0^2/2\mu_0}. \tag{52}$$

Finally, by writing

$$\frac{\omega_{pi}^2}{\omega^2} = \frac{\alpha_i}{2\zeta_i^2} \quad \text{and} \quad \frac{\omega_{pe}^2}{\omega^2} = \frac{k^2}{k_\perp^2}\frac{\alpha_e}{2\zeta_e^2} \tag{53}$$

where

$$\alpha_s \equiv \frac{k_\perp^2 \omega_{ps}^2}{k^2 \omega_{cs}^2 \mu_s} = \frac{2\omega_{ps}^2}{k^2 v_{ts}^2} = \frac{1}{k^2 \lambda_{ds}^2}. \tag{54}$$

(where λ_{ds} is the Debye length for species s) it can be verified that the following set of seven[1] dimensionless parameters

$$\frac{T_i}{T_e}, \quad \frac{u_{de}}{v_{ti}}, \quad \Psi, \quad \beta_e, \quad \frac{\omega_{pe}}{\omega_{ce}}, \quad \frac{m_i}{m_e}, \quad \frac{\nu_e}{\omega_{lh}} \tag{55}$$

completely specify the problem such that, for a given real wavenumber, kr_{ce}, (where r_{ce} is the electron cyclotron radius) we seek the roots, ω/ω_{lh} and γ/ω_{lh} of the dispersion relation[2].

$$\det|D_{ij}| = 0. \tag{56}$$

Similarly, the spatial evolution problem, such as that of the experiments below, is studied by specifying the six parameters listed above and seeking the roots $k_r r_{ce}$ and $k_i r_{ce}$ of Eq. (56) for a given frequency ω/ω_{lh}. It is also worth mentioning that the electrostatic dispersion relation (obtained in the limit $\beta \to 0$) is simply $D_{11} = 0$.

We have used the dispersion tensor derived above in ref. [1] for a detailed study of the nature and dependencies of the dominant microinstability in the MPD accelerator plasma, the lower hybrid current driven instability (LHCDI). The same dispersion tensor was also central to the development of weak turbulence models for the corresponding anomalous transport. We again refer the interested reader to that work.

[1] In the case of a flowing plasma there is an eighth parameter u_f/v_{ti}.

[2] We have found that, for the range of parameters covered in our investigations, cyclotron summations with the seven terms, $n = 0, \pm 1, \pm 2, \pm 3$ are required to reduce the error below 2% [1].

3 Experimental Evidence

As already mentioned, the *main* use of the dispersion tensor derived above is to develop a *theoretical* framework for the description of cross-field microinstabilities in the MPD accelerator plasma and to formulate and calculate the ensuing microturbulent transport. It is compelling, nonetheless, to look for some direct empirical evidence of the existence and importance of current-driven instabilities in the MPD accelerator plasma under nominal operating conditions.

Direct comparison between the above stability theory and experiments present many practical difficulties stemming from the fact that in a steady-state the instabilities are already in a post-saturation condition and may not have fully retained their linear dispersion characteristics.

It is possible, however, to actively excite small amplitude, harmonically rich disturbances, and observe their evolution during the linear stage of their growth (if they happen to grow). Even then, comparison with the linear wave stability theory is still fraught with difficulties due to the many simplifying assumptions. For instance, since the main use of the above theory is to model microturbulent transport, we have adopted a cartesian representation of plane waves, which is not particularly suited for experimental settings where point (or cylindrical) disturbances are excited with small (or cylindrical) probes.

With all these shortcomings in mind, it is still hoped that the observation of waves excited in this manner, may lead to the identification of some linear wave characteristics that are mimicked by the theory. The experiments in this paper present an attempt at such an identification. Any benefits from such attempts must therefore strongly depend on an awareness of how the theory in its limitations can relate to linear wave experiments.

Our focus in this paper will be more on this relationship rather than on any experimental techniques. The experimental techniques, most of which are well-established, have been documented and expounded elsewhere (*cf* Refs. [7] as well as Refs. [8, 9] and the references within).

3.1 Linear Wave Theory Assumptions and Physical Reality

Some of the restrictive assumptions behind the above theory merit a more careful discussion to be better appreciated in the context of experimental reality.

3.1.1 Particle Magnetization

The assumption made in the theory that the electrons are magnetized in the waves while the ions are not can be justified for this experiment since the average magnetic field in the experimental control region was about 380 G (see data below). For the argon plasma the corresponding electron cyclotron radius is about .14 mm and that of the ions is between 4 and 9 cm (for T_i/T_e between 1 and 6), which, when compared to the range of measured wavelengths (between .5 and 3 cm), uphold the validity of the assumption for at least a good part of the observed spectrum.

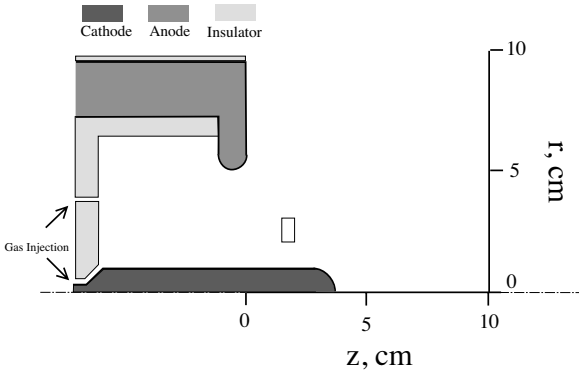

Figure 2: Cross-sectional schematic of Princeton's Full Scale Benchmark Thruster (FSBT). The x-axis is the symmetry axis of the cylindrical device. The small rectangle denotes the position and size of the control region for the experiments.

3.1.2 Infiniteness and Homogeneity

Two restrictive assumptions are those of an infinite and homogeneous plasma. Consequent to these two assumptions is the inability of the formalism to model the stability of the *entire* plasma flow inside the Lorentz force accelerator which, in reality, is subjected to the effects of definite physical boundaries and strong gradients. These two assumptions degrade the formalism from a global description to a local one.

The model can thus only be invoked to describe the conditions at a locale where the local unstable mode is so dominant as not to be overwhelmed by wave reflections off physical boundaries and where the current-driven instability overshadows any gradient-driven instability. A judicious choice of the experimental control region within the discharge can greatly alleviate the limitations imposed by these two assumptions. For the experiments reported here this control volume was therefore chosen to be just outside the device's chamber (as shown in Fig. (2)) thus reducing the importance of reflected waves. Moreover, only forward wave injection (*i.e.* in the positive z direction) was considered so that the absence of downstream boundaries –the flow expanding into vacuum– further reduced the possibility of the excited mode to interact with reflected oscillations. The assumption of infinite plasma is further rendered more benign through the coherence-biased clipping of the wave data, (*cf* Refs. [8, 9]) so that only waves with high coherence are considered[3]. This precaution reduces the chance of including reflected waves in the analysis since such waves would generally have relatively low coherence.

Furthermore, studies where finite plasma effects were included[10, pages 7–10] show that the dispersion curve approaches that of an infinite plasma as the wavelength becomes shorter than the plasma dimension. All the wavelengths considered in the study of this appendix ranged between .5 and 3 cm compared to a plasma dimension on the order of 10 cm.

The homogeneity assumption stipulates that the roles of the temperature and density gradients in the microstability of the plasma are negligible. In reality, every plasma of finite extent *must* support a density gradient. In the flowing, reacting and expanding plasma of the Lorentz force accelerator, temperature and density gradients are omnipresent. These gradients induce diamagnetic drifts that may effect the stability of the plasma. In order to justify the neglect of all terms that are proportional to ∇n_0 and ∇T_0 in the dispersion relation, where n_0 and T_0 are the equilibrium density and temperature, the associated diamagnetic velocities must be much smaller than the measured current velocity. Each gradient contributes a diamagnetic velocity u^*_{de} to the transverse current given by

$$u^*_{de} = \frac{T_e}{m_e \omega_{ce} L} \tag{57}$$

where L is the gradient length scale. In particular, L_n and L_T are the lengths over which the density and temperature are incremented by 100%,

$$L_n \equiv \left| \left(\frac{\nabla n_0}{n_0} \right)^{-1} \right| \tag{58}$$

[3]Coherence is calculated from the oscillation power spectra at the two receiver probes.

$$L_T \equiv \left| \left(\frac{\nabla T_e}{T_e} \right)^{-1} \right|. \tag{59}$$

The total diamagnetic contribution due to both of these effects can then be written as

$$\frac{u^*_{de}}{v_{te}} = \frac{1}{2} \left[\frac{r_{ce}}{L_n} + \frac{r_{ce}}{L_T} \right]. \tag{60}$$

Typical profiles of measured plasma parameters in an MPD accelerator operating at the nominal condition were compiled by *Choueiri*[11]. The compilation shows that the density gradients are significantly stronger than the temperature gradients for the region of interest. Furthermore, the length scale L_n in that region can be estimated to be on the order of one centimeter. From Eq. (60) with an electron cyclotron radius of .14 millimeter we obtain a diamagnetic drift velocity about thirty times smaller than the measured current velocity (measured u_{de}/v_{te} was about .2) thus justifying the neglect of such gradients for our particular experiment.

It can be shown from Faraday's law of induction that the magnitude of the diamagnetic drift scales with $\beta_e u_{de}$. For our particular experiment we measured $\beta_e \simeq .1$ so that gradient effects are not expected to dominate.

It must be cautioned that this situation is not ubiquitous. Indeed, in some locations of the plasma, for instance across the cathode jet, the density gradients can possibly become prevalent and the instability would change from a current-driven to a drift type mechanism. Situations like this prevail in a theta pinch environment, where, as shown by *Gladd*[12] the lower hybrid gradient-drift instability (LHGDI) dominates over LHCDI (or modified two-stream instability). Although *Gladd* showed that LHGDI dominates for gradients whose magnitude is comparable to that of our experiment, his conclusion was based on calculations done with a current velocity $u_{de}/v_{ti} = 4$, which was of the same order as that of the gradient induced drift. In contrast, u_{de}/v_{ti} in our experiment ranged between 20 and 50 (depending on T_i/T_e)[4]. The more recent work of *Migliuolo*[13] showed that the general tendency of finite density gradient effects is to moderately stabilize lower hybrid waves, but he investigated these effects only up to $r_{ci}/L_n = .1$ as relevant to auroral zone and solar wind plasmas[5].

Strictly speaking, the assumption of a homogeneous plasma is not consistent with that of a cross-field current[14]. Indeed, it is common in the literature[15] to invoke the following expression derived from Ampere's law, showing the relation between the cross-field current and the gradients of density and magnetic field,

$$\frac{1}{L_B} = \frac{\omega^2_{pi} j_\perp}{c^2 \omega_{ci} e n_e} + \frac{\beta_i}{2L_n} \tag{61}$$

where L_B is the magnetic field gradient length scale defined similarly to L_n in Eq. (59), c is the speed of light and $j_\perp$ is the cross-field current.

It is obvious from Eq. (61) that no current can exist in the absence of density and magnetic field gradients since for a uniform plasma both L_B and L_n are infinite. It is possible, however, that the stability of some plasma systems can be described to a first order by considering the cross-field current velocity *and* assuming a uniform plasma when the gradients are weak and the particle drift is conditioned by non-gradient effects such as $\boldsymbol{E} \times \boldsymbol{B}$ drifts or externally imposed charged particle beams.

The effects of finite magnetic field gradients were included in the dispersion relation of *Hastings and Niewood*[16] which neglected the effects of ∇n and ∇T and of finite-beta but included electron collisions. Their investigation showed almost no ∇B effect on the real part of the frequency and a modest decrease in growth. These results are, however, inconclusive as far as the MPD accelerator plasma is concerned since the calculations were unfortunately made for gradients with $r_{ce}(m_i/m_e)^{1/2}/2L_B \leq 1$, which correspond to a gradient characteristic length larger than 7 cm for the plasma parameters in ref. [16] and larger than 18 cm for the parameters of our experiment. Both of these values are unrealistic when compared to typical measured magnetic field profiles such as those in ref. [11] and ref. [17, Figure 4-3].

We should also mention that in a nonhomogeneous plasma coupling with electromagnetic modes causes the parallel wavenumber k_y to increase resulting in a destabilization of electrostatic modes. This behavior is the reason why the results of many theories[18, 19] predicting stabilization of LHCDI at finite β values were revised by later theories[20, 15, 21] where the presence of non-homongeneities lead to a further (mostly weak) destabilization of the electromagnetically coupled modes.

[4] A further discrepancy distancing *Gladd*'s conclusions about the dominance of LHGDI from our case is the fact that his calculations assume $\omega_{pe}/\omega_{ce} = 10$ while we have $\omega_{pe}/\omega_{ce} = 100$. An increase in this ratio leads to an increase in the growth as shown in figure 6 of *Gladd*'s paper. This is due to the devaluation of finite Debye effects.

[5] In that work the current was taken to be field aligned, and coupling with electromagnetic modes was allowed.

With all the above said, it remains that a second generation model for the microstability of the MPD accelerator plasma would undoubtedly benefit in accuracy and breadth of applicability from the inclusion of finite gradient effects.

3.1.3 Magnetic Field Curvature and Shear Effects

Neither of these effects were included in the theory. The effects of magnetic shear[22] would be negligible if the discharge is highly symmetric so that only an azimuthal component for the self-induced field B_θ is present. *Hoskins*[23] has undertaken an extensive and careful characterization of the discharge azimuthal symmetry and found that at nominal conditions the discharge becomes very symmetric azimuthally within about 100 μ-secs after gas breakdown. Accordingly the measurements below were made well after 300μ-secs of breakdown to insure discharge symmetry.

Magnetic field curvature effects on plasma waves have not received thorough examination in the literature. It has been recognized that such curvature has a weakly stabilizing effect on the LHGDI[24]. Its neglect in the present study should add to the expectation that the theoretical growth rates represent upper bounds rather than accurate numerical predictions.

3.1.4 Plane Wave Assumption

Since our prime concern while developing a theory for MPD accelerator microstability was its use to formulate anomalous transport models, we opted for the simplifying assumption of plane waves so that a cartesian slab model can be used. Although the cartesian slab model is appropriate for the inclusion of the instability-induced transport in plasma fluid flow codes, it is not very suited to interpret experiments where the disturbances are done with small cylindrical probes. For such disturbances the departure from the plane wave assumption can be significant and can incur errors of the order of λ/R (where λ is the wavelength and R is the wave's radius of curvature) in the dispersion[25]. This restricting assumption must be kept in mind when comparing the wave data below with the theory, especially for the long wavelength part of the observed spectrum.

In particular, for the plasma wave experiment, described below, the distance between the emitter probe and the downstream receiving probe was 1.5 cm while the distance between the two receiver probes was .5 cm, so that we should expect one-third of the spectrum (the long wavelength end) to be most affected by curvature effects since, for these waves, λ/R is slightly larger than unity while it is smaller than one for the shorter wavelength part of the spectrum. This is so because the distance between the emitter probe and the downstream receiver probe is a measure of R while $\lambda_{min} = .5$ cm (since all waves with λ smaller than the distance between the two receivers were actively filtered out by anti-aliasing filters to avoid foldover effects).

Finally, we mention that the theory does not account for the applied electric field that is driving the disturbance nor does it particularly address the the extent to which the (imaginary) line joining the probes corresponds to the direction of the phase velocity. Such effects can be modelled by Fourier analysis of localized point disturbances in a plasma[25], which was not attempted here, thus further distancing the linear theory from probe-excited wave experiments.

With all of the above stated restrictions, it must be apparent by now that linear experiments made to support the above linear wave theory are quite difficult to design, implement and interpret. Indeed, experiments aimed at measurement of the *nonlinear* effects of such instabilities (such as the turbulent fluctuation studies in ref. [8, 9]) are far easier than active linear wave experiments since the former address steady-state (non-evolving) saturated fluctuations instead of tracking the spatial evolution of localized disturbances.

In light of the above mentioned restrictions we should expect from the linear wave experiment described below, at best, a support for the *general* dependences predicted by the theory.

3.2 Plasma Characterization Experiment (PCX)

In order to interface the linear wave theory to localized linear wave experiments, we need to solve the dispersion relation for the plasma parameters corresponding to the conditions at which the wave data were obtained. To this end, the Plasma Characterization Experiment (PCX) uses a cluster of Langmuir and magnetic probes localized within the chosen control volume (*cf* rectangle Fig. (2)).

The test facility has been described in previous theses and reports (see ref. [26] for instance), while the methods and equipment used in PCX have been discussed in refs. [27, 28]. We shall, in this appendix,

focus only on a description of the results.

The experimental errors for all the characterization measurements (PCX) reported here were below 20% (except for the density measurements which depended on the ion temperature whose value was not measured due to the lack of accurate ion temperature measurement techniques). We shall, henceforth, quote only average values of the measured parameters. The errors, however, have been carried in the calculations involved in the normalization of the final data appearing in Figs. (6), (7) and (8) and contribute to the error bars in these figures.

For this particular experiment the accelerator, called the Princeton Full-Scale Benchmark Thruster (FSBT), was operated quasi-steadily with a 1 msec long flat pulse at a total current of 17 kA, and with a 6 g/sec flow rate of argon. The magnetic field was self-induced.

The local electron temperature was measured with an asymmetric double Langmuir probe[28] and found to be at 2.36 eV. The local magnetic field was measured by two magnetic probes[6] located at the inner and outer radii of the experiment's control region. The averaged value of the magnetic field was 382 Gauss. The local axial flow velocity was measured at 10.8 km/sec using the Phase-Flow Velocity Deconvolution (PFVD) technique[29, 30, 31], and was in agreement with estimates based on the electromagnetic thrust law. A local axial component of the current (or drift) velocity u_{de} of 164 km/sec was inferred using the $\nabla \times \boldsymbol{B}$-equation and the magnetic field values measured with the B-probes located at the inner and outer radii of the control region.

The charged number density was inferred from comparing the measured saturation current of the two ends of the double Langmuir probe to an ion current saturation model for a cylindrical probe[28] and averaging the results. An estimate of the ion temperature was needed to accurately determine the value of n_0. Unfortunately, no attempts were made to measure the ion temperature due to the difficulties involved in such a measurement. Consequently, T_i is a free parameter in all our subsequent discussions. Since an accurate inference of n_0 depends on T_i, we have adopted a dependence of n_0 on T_i/T_e based on the measured saturation current and the theory of *Lam*[32]. This dependence is shown in Fig. (3) where a simpler theory of collection at the Bohm velocity is also shown for reference.

[6]The magnetic probes were built by Andrew Hoskins for his discharge symmetry studies in ref. [23]. Their calibration and description are described in that reference.

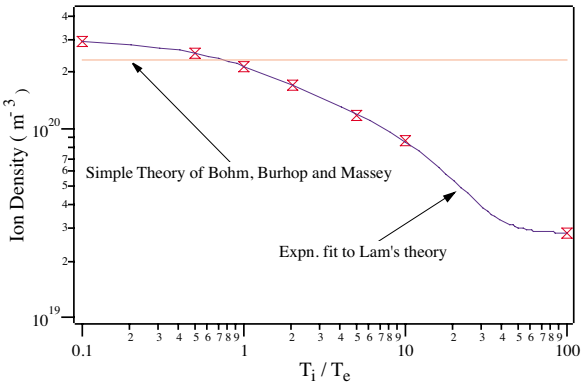

Figure 3: Ion density dependence on the ion temperature based on measurement of probe saturation current and *Lam*'s theory[32]. The simpler, T_i-independent estimate based on the Bohm velocity is also shown for reference.

Since other parameters of the theory such as ω_{pe}/ω_{ce} and ν_e/ω_{lh} depend on the number density, the n_0–T_i dependence shown in Fig. (3) was carried in the calculations. To cover a plausible range for the free parameter T_i, we have chosen three values for T_i/T_e , 1, 3 and 6, for our calculations.

A characterization of the local plasma under the above described conditions is illustrated in Figs. (4) and (5) , which were obtained using the Princeton Plasma Characterization Software (PPrinCesS)[7]. The characterization set shown in these figures was obtained for $T_i/T_e = 1$.

3.3 Plasma Wave Experiment (PWX)

In PWX (described in Refs. [27, 33, 28]) a double E-probe (symmetric double probe with cylindrical 5-mil wires) is connected to a plasma wave driver (which supplies low rf-power below the thermal level of the plasma, thus insuring initially linear waves), placed at the upstream end of the control region shown in Fig. (2) and used to excite a harmonically rich disturbance in the local electric field. Two similar re-

[7]The Princeton Plasma Characterization Software (PPrinCesS) is an interactive stand-alone application for the Macintosh developed at the Electric Propulsion and Plasma Dynamics Lab. This interactive software calculates and plots various natural and collisional time and length scales of a plasma (only a subset of which is shown here) from a small number of input parameters. The utility is in the public domain and available free-of-charge upon request.

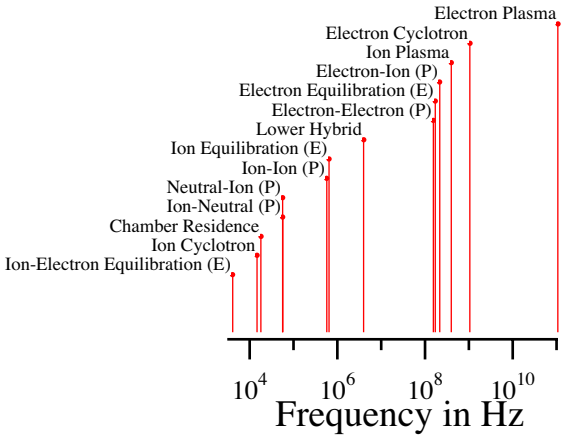

Figure 4: Output of PPrinCesS showing the frequency scale ordering for the parameters of this experiment.

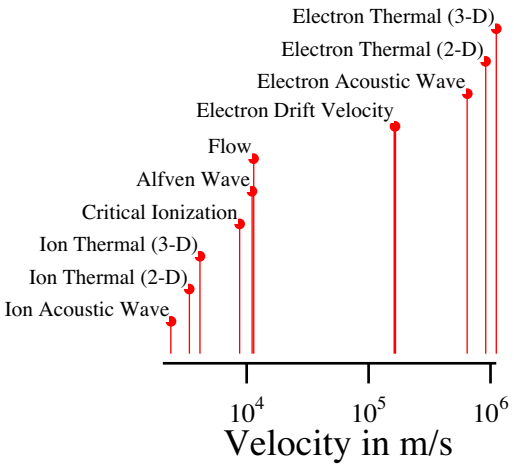

Figure 5: Output of PPrinCesS showing the velocity scale ordering for the parameters of this experiment.

ceiver probes, with 5 mm axial separation, are aligned along the accelerator axis at the downstream end of the control region. The two receiver probes are passively biased to draw ion saturation current and are thus sensitive to the local oscillations in the plasma density (hence the oscillations of the electric field). The receiver probes are connected to digital recorders through low attenuation (RG-217/U) cables. Special care was taken to insure that the frequency response of the entire system is flat within the spectrum of interest (up to 10 MHz) and that no spurious phase-shifts or relative attenuation existed between the separate probe circuits. Second-order low-pass filters with a cut-off frequency around 5 Mhz were used (while the Nyquist frequency was at 10 MHz), in order to avoid aliasing. A similar set-up was recently replicated by *Tilley*[8, 9] for PWX measurements in a low-power accelerator and is described in more detail in that reference along with the standard data-reduction techniques. The standard error analysis used to estimate the contribution of signal analysis to the error bars shown in the figures below was also described in that reference and the literature cited within.

A fast Fourier algorithm (FFT) was used for the frequency-domain analysis. A Hanning window function was used to reduce "leakage" effects while a frequency-domain averaging technique with interloping bands of five data-points each was used to reduce the noise. A cross-coherence spectrum was calculated from signal analysis theory using the two digitally recorded signals at the receivers and is shown in Fig. (6).

It is very clear from this spectrum that active wave injection can result in a highly coherent reception for a significant part of the spectrum. The coherence drops significantly above 4 Mhz due to low-pass filtering. The cause of low coherence below 1.2 MHz is probably related to collisional damping. All subsequent data analysis was done with the highly coherent part of the spectrum (1.2 MHz $\leq f \leq$ 4 MHz) only. From the phase-spectrum (obtained by multiplying the two power spectra), and knowing the distance between the probes, the wavelength-spectrum can readily be calculated. This is essentially the real part of the dispersion relation. Similarly, the ratio of the magnitude of the two intensity spectra yields the attenuation-spectrum, which is essentially the imaginary part of the dispersion relation. Not surprisingly, the highly coherent part of the spectrum corresponded to growing (unstable) disturbances.

The resulting data were then normalized using measured plasma parameters from PCX. In particular, the wave number was normalized by the electron cyclotron radius while the frequency was cast in units of the lower hybrid frequency. The final results with the estimated error bars are plotted in Figs. (7) and (8) along with the numerical spatial evolution solutions of the dispersion relation (Eq. (56)), obtained for the same parameters and for the three values of

the free parameter T_i/T_e[8].

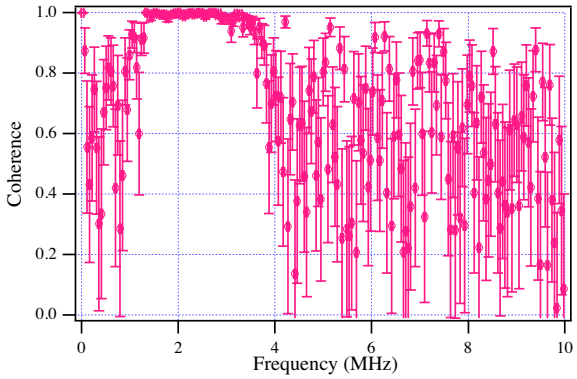

Figure 6: Cross-coherence spectrum for PWX showing highly coherent oscillations in the 1.2–4 MHz frequency range.

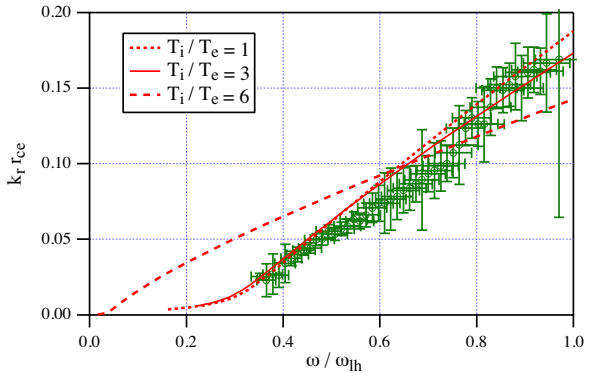

Figure 7: Measured normalized wavenumber plotted as a function of the measured frequency in units of lower hybrid frequency. The curves represent theoretical solutions at three values of the free-parameter T_i/T_e.

We note from Fig. (7) that the magnitude and trend of the real part of the dispersion relation is, in general, correctly predicted by theory. This is especially the case for lower values of the free parameter T_i/T_e. The agreement is far worse, as should be expected, for the imaginary part of the dispersion since spatial growth rates of the unstable waves are much more sensitive to the plasma parameters than their phase. Unfortunately, the theory, in this region of parameter-space, was very sensitive to the free-parameter T_i/T_e as clearly seen in Fig. (8). It must be said, in this context, that the choice of $T_i/T_e = 3$ was not done arbitrarily or *a priori*; it was rather the value of the free-parameter that gave the best agreement with theory. Even for this value it is clear from the plot that the lower frequency part of the unstable spectrum is not well predicted and the frequency at maximum growth (maximum negative k_i) is somewhat underpredicted. Specifically, the theory predicts maximum growth at about half the lower hybrid frequnecy (for $T_i/T_e = 3$) while the experimental value is around $.8\omega_{lh}$. We do not have any concise physical arguments that could explain this discrepancy. We note, however, that the discrepancies might be related to the fact that longer wavelengths suffer most from the plane wave assumption. Also, the longer wavelength oscillations had the strongest spatial growth rate per unit wavelength, which threatens the validity of the *linear* wave assumption.

It is relevant, here, to remember all of the restrictions listed in the preceding section about the applicability of such a theory to an active wave injection experiment of this kind. It is obvious that any more quantitative description of active linear wave exper-

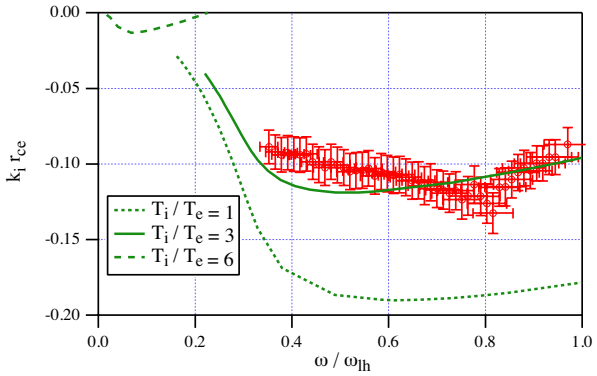

Figure 8: Measured normalized spatial growth plotted as a function of the measured frequency in units of lower hybrid frequency. The curves represent theoretical solutions at three values of the free-parameter T_i/T_e.

[8]The value of Ψ needed by the theory is difficult to estimate for that particular probe configuration. Luckily, the results were obtained under the conditions of strong collisionality for which the phase spectrum becomes isotropic[1]. Consequently, the solutions were weakly dependent on Ψ and a value of 10 was arbitrarily chosen. Had the collisionality been weak, Ψ would have been another free parameter in the problem.

iments must rely on a specialized theoretical formulation of the problem of localized externally driven disturbances in plasmas. Comparison of such future theories with experiments would most probably still require accurate estimates of the ion temperature. Moreover, the problem of accurate ion temperature measurement looms as an outstanding experimental question in the context of more quantitative MPD accelerator plasma studies.

4 Conclusions

The dielectric tensor for a magnetoactive, current-carrying, collisional and finite-beta flowing plasma such as that of the MPD accelerator was derived using kinetic theory without making the electrostatic assumption. Although the resulting description is best suited for a theoretical parametric investigation of microinstabilities and anomalous transport in the MPD accelerator plasma as done in ref. [1], an attempt was made to design and conduct a wave experiment that can be compared to the theory. The difficulties in designing an experiment that can be reconciled with the assumptions of the theory were addressed. Local plasma parameter measurements were used to solve the dispersion relation for both phase and spatial growth spectra and the solutions were compared to the same spectra measured in the discharge. Waves near the lower hybrid frequency were found to have a linear stage of spatial growth and hence are unstable. Although the real part of the measured dispersion compares favorably to the theory, the imaginary part was found to be sensitive to the ion temperature which was unknown. Good agreement can be reached by assuming $T_i/T_e = 3$ which is not an unreasonable value. The general agreement underscores the importance of the Generalized Lower Hybrid Drift Instability (GLHDI) to the MPD accelerator plasma.

References

[1] E.Y. Choueiri. *Electron-Ion Streaming Instabilities of an Electromagnetically Accelerated Plasma*. PhD thesis, Princeton University, Princeton, NJ, USA, 1991.

[2] G. Caldo, E.Y. Choueiri, A. J. Kelly, and R. G. Jahn. An MPD code with anomalous transport. In 22^{nd} *International Electric Propulsion Conference*, Viareggio, Italy, 1991. IEPC-91-101.

[3] E.Y. Choueiri, A. J. Kelly, and R. G. Jahn. Current-driven plasma acceleration versus current-driven energy dissipation part I : Wave stability theory. In 21^{st} *International Electric Propulsion Conference*, Orlando, Florida, 1990. AIAA-90-2610.

[4] P.L. Bhatnagar, E.P. Gross, and M. Krook. Collision models in gases. *Physical Reviews*, 94, 1954.

[5] J.D. Callen and G.E. Guest. Electromagnetic effects on electrostatic modes in a magnetized plasma. *Nuclear Fusion*, 13:87–110, 1973.

[6] C.L. Chang, H.K. Wong, and C.S. Wu. Electromagnetic instabilities attributed to a cross-field ion drift. *Physical Review Letters*, 65(9):1104–1107, 1990.

[7] E.Y. Choueiri. Plasma wave studies. Contribution to the following Bimonthly Progress Reports of the Electric Propulsion and Plasma Dynamics Laboratory. Technical Report MAE 1692.27, MAE 1776.03, MAE 1776.11, MAE 1776.14, Electric Propulsion and Plasma Dynamics Laboratory, Princeton University, 1986-1988.

[8] D.L. Tilley. An investigation of microinstabilities in a kW level self-field MPD thruster. Master's thesis, Princeton University, Princeton, NJ, USA, 1991.

[9] D.L. Tilley, E.Y. Choueiri, A.J. Kelly, and R.G. Jahn. An investigation of microinstabilities in a kW level self-field MPD thruster. In 22^{nd} *International Electric Propulsion Conference*, Viareggio, Italy, 1991. IEPC-91-122.

[10] K.W. Gentle. Plasma waves and echoes. In R.H. Lovberg and H.R. Griem, editors, *Methods of Experimental Physics, Plasma Physics*, chapter 1. Academic Press, Inc., New York, 1970. Volume 9, Part A.

[11] E.Y. Choueiri. Theoretical modelling. Contribution to the August Progress Report of the Electric Propulsion and Plasma Dynamics Laboratory. Technical Report MAE 1692.23, EPPDyL, Princeton University, 1986.

[12] N.T. Gladd. The lower hybrid drift instability and the modified two stream instability in high density pinch environments. *Plasma Physics*, 18:27–40, 1976.

[13] S. Migliuolo. Lower hybrid waves in finite-β plasmas, destabilized by electron beams. *Journal of Geophysical Research*, 90(A1):377–385, 1985.

[14] F. Perkins, 1990. Princeton, University. Personal communication.

[15] J.B. Hsia, S.M.Chu, M.F. Hsia, R.L. Chou, and C.S. Wu. Generalized lower-hybrid-drift instability. *Physics of Fluids*, 22(9):1737–1746, 1979.

[16] D. Hastings and E. Niewood. Theory of the modified two stream instability in an MPD thruster. In 25^{th} *Joint Propulsion Conference*, Monterey, CA, USA, 1989. AIAA-89-2599.

[17] M.J. Boyle. *Acceleration Processes in the Quasi-Steady Magnetoplasmadynamic Discharge*. PhD thesis, Princeton University, Princeton, NJ, USA, 1974.

[18] J.B. McBride and E. Ott. Electromagnetic and finite-β_e effects on the modified two stream instability. *Physics Letters*, 39A(5):363–364, 1972.

[19] A.I. Paytak and V.L. Sizonenko. Instabilities in a finite-β plasma with transverse current. Part I. *Soviet Physics, Technical Physics*, 19(5):635–639, 1974.

[20] D.S. Lemons. *Cross Field Current Instabilities in a Vlasov Plasma*. PhD thesis, College of William and Mary, Williamsburg, VA, USA, 1977.

[21] C.S. Wu, Y.M. Zhou, S.T. Tsai, and S.C. Guo. A kinetic cross-field streaming instability. *Physics of Fluids*, 26(5):1259–1267, 1983.

[22] N.A. Krall. Shear stabilization of lower hybrid drift instabilities. *Physics of Fluids*, 20(2):311–312, 1977.

[23] W.A. Hoskins. Asymetric discharge patterns in the MPD thruster. Master's thesis, Princeton University, Princeton, NJ, USA, 1990.

[24] L.J. Rahal and S.P. Gary. Lower hybrid density drift instability with magnetic curvature. *Physics of Fluids*, 24(8):1588–1589*, 1981.

[25] S.H. Lam, 1991. Princeton University. Personal communication.

[26] M. Wolff. A high performance MPD thruster. Master's thesis, Princeton University, Princeton, NJ, USA, 1983.

[27] E.Y. Choueiri, A.J. Kelly, and R.G. Jahn. MPD thruster instability studies. In 19^{th} *International Electric Propulsion Conference*, Colorado Springs, CO, USA, 1987. AIAA-87-1067.

[28] E.Y. Choueiri. Plasma wave studies. Contribution to the January/February Bimonthly Progress Report of the Electric Propulsion and Plasma Dynamics Laboratory. Technical Report MAE 1776.11, EPPDyL, Princeton University, 1988.

[29] E.Y. Choueiri. Plasma wave studies. Contribution to the following Bimonthly Progress Reports of the Electric Propulsion and Plasma Dynamics Laboratory. Technical Report MAE 1692.11, MAE 1776.12, Electric Propulsion and Plasma Dynamics Laboratory, Princeton University, 1988.

[30] K.D. Diamant. Plasma wave studies. Contribution to the following Bimonthly Progress Reports of the Electric Propulsion and Plasma Dynamics Laboratory. Technical Report MAE 1776.27, MAE 1776.28, MAE 1776.29, Electric Propulsion and Plasma Dynamics Laboratory, Princeton University, 1990-1991.

[31] K.D. Diamant, D.L. Tilley, E.Y. Choueiri, A. J. Kelly, and R. G. Jahn. Velocity measurement in the plume of an MPD thruster using injected plasma waves. In 22^{nd} *International Electric Propulsion Conference*, Viareggio, Italy, 1991. IEPC-91-049.

[32] S.H. Lam. Unified theory for the langmuir probe in a collisionless plasma. *Physics of Fluids*, 8(1):73–87, 1965.

[33] E.Y. Choueiri, A. J. Kelly, and R. G. Jahn. Current-driven instabilities of an electromagnetically accelerated plasma. In 20^{th} *International Electric Propulsion Conference*, Garmisch-Partenkirchen, W. Germany, 1988. AIAA-88-042.